

Coarse Graining in Block Copolymer Films

Yoav Tsori

*Department of Chemical Engineering,
Ben-Gurion University of the Negev,
P.O. Box 653, 84105 Beer-Sheva, Israel*

David Andelman

*School of Physics and Astronomy
Raymond and Beverly Sackler Faculty of Exact Sciences
Tel Aviv University, Ramat Aviv, Tel Aviv 69978 Israel*

We present few ordering mechanisms in block copolymer melts in the coarse-graining approach. For chemically homogeneous or modulated confining surfaces, the surface ordering is investigated above and below the order-disorder temperature. In some cases the copolymer deformation near the surface is similar to the copolymer morphology in bulk grain boundaries. Block copolymers in contact with rough surfaces are considered as well, and the transition from lamellae parallel to perpendicular to the surface is investigated as a function of surface roughness. Finally, we describe how external electric fields can be used to align block copolymer meso-phases in a desired direction, or to induce an order-order phase transition, and dwell on the role of mobile dissociated ions on the transition.

keywords: block copolymers, confinement, electric fields, phase transitions

PACS numbers:

INTRODUCTION

Block copolymers (BCP) are heterogeneous polymers where each polymer chain is composed of several chemically distinct homopolymer blocks, connected together by a covalent bond. These polymeric systems exhibit fascinating structures in the nanometer scale and can be created by self-assembly from solutions or the melt state [1, 2].

In addition, BCP are composite materials that have many applications. For example, by connecting together a stiff (rod-like) block with a flexible (coil) block, one can obtain a material which is rigid, but not brittle [3, 4]. Moreover, the interplay between flexibility and toughness can be controlled by temperature. Different chain architecture (ring or star-like) may lead to novel mechanical and flow properties [5]. In addition, BCP have many industrial uses because the length scales involved are smaller or comparable to the wavelength of light. These applications include waveguides, photonic band gap materials and other optoelectronic devices [6] and dielectric mirrors [7].

Our prime concern in this mini-review are melts of BCP above the glass transition. However, it is worthwhile mentioning that BCP also exhibit interesting properties upon cooling below the glass transition into a solid state. Some BCP may undergo crystallization of one or more components that is accompanied by strong structural changes, while other BCP systems stay in the vitrified state upon cooling.

In the molten state, because of competition between enthalpy and entropy, at high temperatures the BCP

melt behaves as a disordered fluid, while at low temperatures the macroscopic phase separation is hindered because the two (or more) immiscible sub-chains cannot be detached from each other as they try to phase separate due to block incompatibility. Hence, BCP'S phase separate into a variety of micro-ordered structures, with characteristic size depending on the BCP chain length and other system parameters [1, 2]. The morphology and structure of the prevailing phase depend on the lengths of constituent sub-chains (also called blocks), the chemical interactions between the blocks, the temperature and the chain architecture. The BCP micro-domain size ranges from about 10 to several hundreds nanometers.

A typical example of a well-studied di-BCP, polystyrene-polyisoprene (PS-PI), is shown in Fig. 1 [8]. As temperature is cooled below the order-disorder temperature (ODT), the disorder melt of chains micro-phase separates into one of the meso-phases: lamellar, hexagonal, body centered cubic (bcc) or gyroid.

The present paper reviews several mechanisms that can be used to achieve a desired ordering and orientation in thin films of BCP. The simple analytical model is presented in Sec. , valid in the weak segregation limit (WSL). We consider in Sec. BCP'S above the ODT point and in contact with chemically patterned surfaces. The polymer density is given as a function of a pre-designed and fixed chemical pattern on the surface. Thin films of di-BCP'S below the ODT confined between two flat and parallel surfaces are investigated in Sec. . We find that for a one-dimensional chemical surface pattern, the lamellae are tilted with respect to the parallel surfaces. If the surface and lamellar periodicities are equal, the

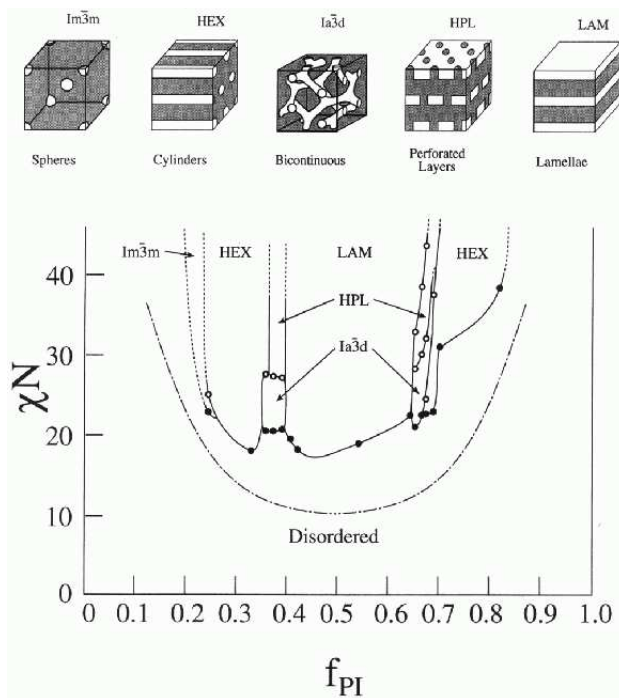


FIG. 1: χN versus f_{PI} phase diagram for PI-PS diblock copolymers. The dash-dot curve is the mean field prediction for the ODT. Solid curves have been drawn to delineate the different phases observed but might not correspond to precise phase boundaries. Five different ordered microstructures (shown schematically) have been observed for this chemical system. Adapted with permission from ref [8].

lamellae are formed perpendicular to the surfaces. We relate the orientation phenomenon to the formation of tilt boundary (chevrons) defects in bulk lamellar phases. Beside chemically heterogeneous surfaces, rough surfaces are investigated in Sec. , and a simple explanation to the parallel to perpendicular transition in these system as function of surface roughness is proposed. Alignment of confined lamellae by external electric fields is studied in Sec. . It is shown that because different polymers have different values of the dielectric constant, the electrostatic energy favors an orientation of lamellae in a direction perpendicular to the confining electrodes. This electrostatic tendency can be used to overcome interfacial interactions with the bounding electrodes and align structures in a desired direction.

THE MODEL

Let us consider first a simple free energy expression for A/B di-BCP melt. With the definition of the order parameter $\phi(\mathbf{r}) \equiv \phi_A(\mathbf{r}) - f$ as the local deviation of the A monomer concentration from its average, the bulk free

energy can be written as [9, 10]:

$$\frac{Nb^3 F_b}{k_B T} = \int \left\{ \frac{1}{2} \tau \phi^2 + \frac{1}{2} h (\nabla^2 \phi + q_0^2 \phi)^2 + \frac{1}{6} \Lambda \phi^3 + \frac{u}{24} \phi^4 \right\} d^3 r \quad (1)$$

$d_0 = 2\pi/q_0$ is the fundamental periodicity in the system, and is expressed by the polymer radius of gyration R_g through $q_0 \simeq 1.95/R_g$. The parameter $\tau = 2\rho N(\chi_c - \chi)$ measures the distance from the critical point ($\tau = 0$) in terms of the Flory parameter $\chi \sim 1/T$. At the critical point (or equivalently the ODT) $\chi_c \simeq 10.49/N$. In addition, b is the Kuhn statistical segment length, $h = 1.5\rho c^2 R_g^2/q_0^2$ and $\rho = 1/Nb^3$ is the chain density per unit volume. Λ and u are the three- and four-point vertex functions calculated by Leibler [9].

For simplicity we will restrict most (but not all) the discussion below to lamellar phases of symmetric BCP'S. This allows us to simplify the above free energy by considering only the symmetric case: $f = \frac{1}{2}$ and the cubic Λ -dependent term drops out. In addition, we set for convenience $c = u/\rho = 1$ throughout the paper. However, in Sec. where we treat the bcc to hexagonal transition we will consider also the cubic term in the free energy as it is indispensable to describe asymmetric phases.

BCP'S [11, 12, 13] and other systems with spatially modulated phases [14] have been successfully described by Eq. (1) or similar forms of free energy functionals. The free energy, Eq. (1), describes a system in the disordered phase having a uniform $\phi = 0$ for $\chi < \chi_c$ (positive τ), while for $\chi > \chi_c$ (negative τ), the system is in the lamellar phase for $f = \frac{1}{2}$, $\Lambda = 0$, and can be described approximately by a single q -mode $\phi = \phi_L \exp(i\mathbf{q}_0 \cdot \mathbf{r})$. The amplitude of the sinusoidal modulations is given by $\phi_L^2 = -8\tau/u$. The validity of Eq. (1) is limited to a region of the phase diagram close enough to the critical point where the expansion in powers of ϕ and its derivatives is valid, but not too close to it, because then critical fluctuations become important [15, 16]. This limit employed hereafter is called the weak segregation limit (WSL).

DISORDERED BCP'S IN CONTACT WITH CHEMICALLY PATTERNED SURFACES

The presence of chemically heterogeneous but otherwise flat surface is modeled by adding short-range surface interactions to the free energy of the form,

$$F_s = \int [\sigma(\mathbf{r}_s)\phi(\mathbf{r}_s) + \tau_s \phi^2(\mathbf{r}_s)] d^2 \mathbf{r}_s + const. \quad (2)$$

The integration is carried out over the position of the confining surfaces parameterized by the vector \mathbf{r}_s . The surface field is $\sigma(\mathbf{r}_s) \equiv \gamma_{AS} - \gamma_{BS}$, where γ_{AS} and γ_{BS} are the interfacial interactions of the A and B blocks with

the surface, respectively. Furthermore, σ has an arbitrary but fixed spatial variation and is coupled linearly to the BCP surface concentration $\phi(\mathbf{r}_s)$. Preferential adsorption of the A block ($\phi > 0$) onto the *entire* surface is modeled by a constant $\sigma < 0$ surface field, resulting in parallel-oriented layers (a perpendicular orientation of the chains). One way of producing such a surface field in experiments is to coat the substrate with random copolymers [17, 18]. If the pattern is spatially modulated, $\sigma(\mathbf{r}_s) \neq 0$, then the A and B blocks are attracted to different regions of the surface. The coefficient of the ϕ^2 term in Eq. (2) is taken to be a constant surface correction to the Flory parameter χ [19, 20]. A positive τ_s coefficient corresponds to a suppression of surface segregation of the A and B monomers.

One surface

For simplicity we consider first BCP'S confined by one surface located at $y = 0$ as is depicted in Fig. 2 (a). A generalization to two parallel surfaces is not difficult and will be given later. The surface chemical pattern $\sigma(\mathbf{r}_s) = \sigma(x, z)$ can be decomposed in terms of its q -modes

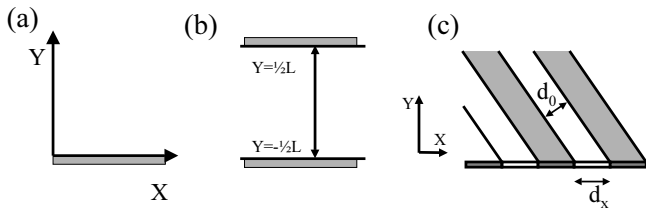


FIG. 2: Schematic illustration of the coordinate system for BCP'S confined by one [part (a)] or two [part (b)] planar and parallel surfaces. (c) Lamellae are formed tilted with respect to the surface if the surface periodicity d_x is larger than the natural one d_0 .

$$\sigma(x, z) = \sum_{\mathbf{q}} \sigma_{\mathbf{q}} e^{i(q_x x + q_z z)} \quad (3)$$

where $\mathbf{q} = (q_x, q_z)$, and $\sigma_{\mathbf{q}}$ is the mode amplitude. Similarly, ϕ can be written as a sum

$$\phi(\mathbf{r}) = \sum_{\mathbf{q}} \phi_{\mathbf{q}}(y) e^{i(q_x x + q_z z)} \quad (4)$$

Close to the ODT the free energy is stable to second order in ϕ , and higher order terms (i.e. the ϕ^4 term) can be neglected. Then $\phi(\mathbf{r})$ is inserted into Eq. (1) and an integration over the x and z coordinates is carried out. Minimization with respect to $\phi_{\mathbf{q}}(y)$ yields the Euler-Lagrange equation

$$\left[\tau/h + (q^2 - q_0^2)^2 \right] \phi_{\mathbf{q}} + 2(q_0^2 - q^2) \phi_{\mathbf{q}}'' + \phi_{\mathbf{q}}'''' = 0 \quad (5)$$

Note that the equation is linear and that the Fourier harmonics $\phi_{\mathbf{q}}$ are not coupled. The boundary conditions are rather complicated because they couple the value of the amplitude and its derivatives at the surface. They result from minimization of the full free energy expression, Eqs. (1) and (2)

$$\phi_{\mathbf{q}}''(0) + (q_0^2 - q^2) \phi_{\mathbf{q}}(0) = 0 \quad (6)$$

$$\sigma_{\mathbf{q}}/h + 2\tau_s \phi_{\mathbf{q}}(0)/h + (q_0^2 - q^2) \phi_{\mathbf{q}}'(0) + \phi_{\mathbf{q}}'''(0) = 0 \quad (7)$$

Since Eq. (5) is linear, its solution is a sum of exponentials,

$$\phi_{\mathbf{q}}(y) = A_{\mathbf{q}} \exp(-k_{\mathbf{q}} y) + B_{\mathbf{q}} \exp(-k_{\mathbf{q}}^* y) \quad (8)$$

where the modulation constant $k_{\mathbf{q}}$ and the amplitude $A_{\mathbf{q}}$ are given by

$$k_{\mathbf{q}}^2 = q^2 - q_0^2 + i\sqrt{\tau/h} \quad (9)$$

$$A_{\mathbf{q}} = -\sigma_{\mathbf{q}} \left(4\tau_s + 2\text{Im}(k_{\mathbf{q}}) \sqrt{\tau h} \right)^{-1}$$

In the above $\text{Re}(k_{\mathbf{q}}) > 0$ ensuring that $\phi_{\mathbf{q}} \rightarrow 0$ as $y \rightarrow \infty$. This restricts the solution $\phi_{\mathbf{q}}$ to be a sum of only two (out of four) exponential terms.

The two lengths, $\xi_q = 1/\text{Re}(k_{\mathbf{q}})$ and $\lambda_q = 1/\text{Im}(k_{\mathbf{q}})$, correspond to the exponential decay and oscillation lengths of the q -modes, respectively. For fixed χ , ξ_q decreases and λ_q increases with increasing q . Close to the ODT and for $q > q_0$ we find finite ξ_q and $\lambda_q \sim (\chi_c - \chi)^{-1/2}$. However, all q -modes in the band $0 < q < q_0$ are equally “active”, i.e., these modes decay to zero very slowly in the vicinity of the ODT as $y \rightarrow \infty$: $\xi_q \sim (\chi_c - \chi)^{-1/2}$ and λ_q is finite. Therefore, the propagation of the surface imprint (pattern) of q -modes with $q < q_0$ into the bulk can persist to long distances, in contrast to surface patterns with $q > q_0$ which persist only close to the surface. The $q = q_0$ mode has both lengths ξ_q, λ_q diverging as $(\chi_c - \chi)^{-1/4}$ for $\chi \rightarrow \chi_c$.

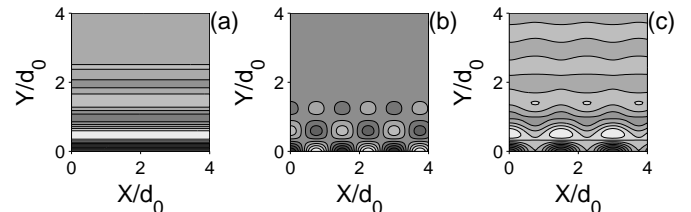


FIG. 3: A BCP melt confined by one surface at $y = 0$. B-monomer density is high in dark regions, while A monomers are in light regions. In (a) the surface is uniform, $\sigma = 0.3$ and in (b) it has stripes given by $\sigma = 0.3 \cos(\frac{2}{3} q_0 x)$. The “combined” effect is shown in part (c) where $\sigma = 0.3 + 0.3 \cos(\frac{2}{3} q_0 x)$ has a uniform and modulated part. The Flory parameter is $N\chi = 10.2$, $\tau_s = 0$ and lengths in the x and z directions are scaled by the lamellar period d_0 . Adapted from ref [21].

In Fig. 3 we give examples of the polymer morphologies in the case of three simple surface patterns. A uniform surface [in (a), $\sigma = \sigma_0$ is constant] causes exponentially decaying density modulations to propagate in the y -direction. A striped surface [in (b), $\sigma = \sigma_q \cos(qx)$] creates a disturbance that is periodic in the x -direction, which decays exponentially in the y -direction. The combined surface pattern [in (c), $\sigma = \sigma_0 + \sigma_q \cos(qx)$] induces density modulations which are the sum of the ones in (a) and (b).

A more complex chemical pattern, shown in Fig. 4 (a), consists of V shaped stripes on the $y = 0$ surface. The polymer density in parallel planes with increasing distance from the surface is shown in (b) and (c). Note how the frustration induced by the tips of surface chemical pattern [in (a)] is relieved as the distance from the surface increases. Similar morphology is observed when two grains of lamellar phase meets with a tilt angle, creating a tilt grain boundary in bulk systems.

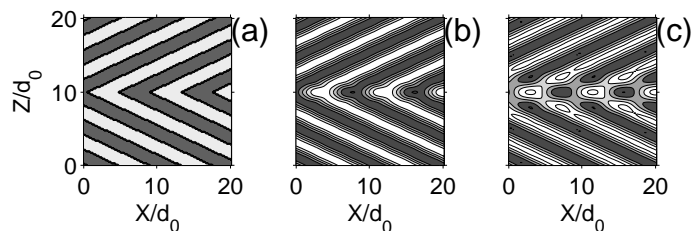


FIG. 4: Propagation of surface pattern into the bulk. The surface pattern in the $y = 0$ plane is shown in (a), where white (black) show regions preferring A (B) monomers. Parts (b) and (c) are contour plots of the polymer density at $y = 3d_0$ and $y = 8d_0$, respectively. $N\chi = 9.5$ and $\tau_s = 0$. Adapted from ref [21].

Two confining surfaces

Our treatment of confined BCP'S can be easily generalized to the case of two flat parallel surfaces [22]. The governing equation is still Eq. (5), but now there are four boundary conditions instead of the two in Eqs. (6) and (7). Figure 5 shows how two simple surface patterns can be used to achieve a complex three-dimensional polymer morphology, even though the melt is in its bulk disordered phase. The stripes on the two surfaces are rotated by 90° with respect to each other. A symmetric “checker-board” morphology appears in the mid-plane.

Up to this point, the BCP melt was assumed to be in its bulk disordered phase (above the bulk ODT point). When a melt in the lamellar phase (below ODT) is confined in a thin film, the morphology is dictated by a complex interplay between the natural periodicity and the imposed film thickness.

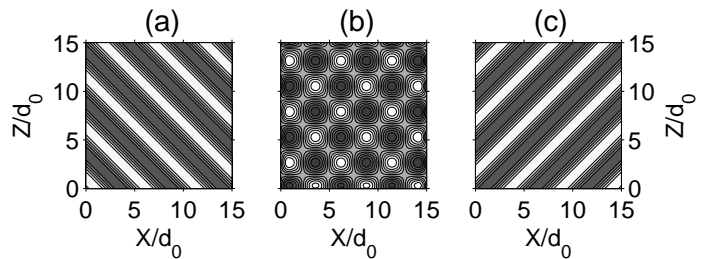


FIG. 5: BCP melt confined by two flat parallel striped surfaces, depicted in parts (a) and (c), and located at $y = -d_0$ and $y = d_0$, respectively. The melt morphology in the mid-plane ($y = 0$) is shown in part (c). The Flory parameter is $N\chi = 9$ and $\tau_s = 0$. Adapted from ref [22].

LAMELLAR BCP BETWEEN TWO CHEMICALLY PATTERNED SURFACES

In this section we describe the ordering of lamellar BCP's confined by one or two surfaces. The phase behavior of thin BCP films in the lamellar phase subject to *uniform* surface fields has been investigated experimentally [23] and theoretically [19, 24, 25, 26, 27, 28, 29], and was found to consist of parallel, perpendicular and mixed lamellar phase. The latter phase has parallel lamellae extending from one surface, which are jointed in a T-junction defect with perpendicular lamellae extending from the opposite surface [30, 31]. At a given inter-surface spacing, increasing the (uniform) surface interactions promotes a parallel orientation with either A-type or B-type monomers adsorbed onto the surface. However, if the spacing L between the surfaces is incommensurate with the lamellar periodicity, or the incompatibility χ is increased, a perpendicular orientation is favored [32].

In the treatment given below, a new effect can be observed when the surfaces are taken to be non-uniform, “striped”, with regions of alternating preferences to the A and B blocks [see Fig. 2 (c)] [33]. The stripe periodicity d_x is assumed to be larger than the natural (bulk) periodicity, $d_x > d_0$, and the stripes are modeled by

$$\sigma(x, z) = \sigma_q \cos(q_x x) \quad (10)$$

and are translational invariant in the z -direction. The surface q -mode is $q_x = 2\pi/d_x < q_0$.

Contrary to the system above the ODT, a linear response theory assuming small order parameter as a response to the surface field is inadequate here, since the bulk phase has an inherent spatially varying structure. The surface effects are contained in the correction to the order parameter

$$\delta\phi(\mathbf{r}) \equiv \phi(\mathbf{r}) - \phi_b(\mathbf{r}) \quad (11)$$

where ϕ_b is a “tilted” bulk lamellar phase given by

$$\phi_b = -\phi_L \cos(q_x x + q_y y) \quad (12)$$

$$q_x = q_0 \cos \theta, \quad q_y = q_0 \sin \theta, \quad (13)$$

The bulk ordering is depicted schematically as tilted lamellae in Fig. 2 (c). For the correction order parameter $\delta\phi$ we choose

$$\delta\phi(x, y) = g(y) \cos(q_x x). \quad (14)$$

This correction describes a lamellar ordering perpendicular to the surface, and commensurate with its periodicity $d_x = 2\pi/q_x$. The overall morphology of the lamellae is a superposition of the correction field $\delta\phi$ with the tilted bulk phase, having a periodicity d_0 . The region where the commensurate correction field $\delta\phi$ is important is dictated by the amplitude function $g(y)$. The total free energy $F = F_b + F_s$ is now expanded about its bulk value $F[\phi_b]$ to second order in $\delta\phi$. The variational principle with respect to $g(y)$ yields a master equation:

$$[A + C \cos(2q_y y)] g(y) + Bg''(y) + g''''(y) = 0, \quad (15)$$

with parameters A , B and C given by:

$$A = -\tau/h + q_y^4, \quad B = 2q_y^2, \quad C = -\tau/h. \quad (16)$$

This linear equation for $g(y)$ is similar in form to Eq. (5) describing the density modulation of a BCP melt in the disordered phase. The lamellar phase is non-uniform and this results in a y -dependency of the term in square brackets. The above equation is readily solved using the proper boundary conditions (for more details see refs. [20, 34]).

In Fig. 6 we present results for a BCP melt confined by one sinusoidally patterned surface, $\sigma(x) = \sigma_q \cos(q_x x)$, with no average preference to one of the blocks, $\langle \sigma \rangle = 0$, for several values of surface periodicity d_x and for fixed value of the Flory parameter $\chi > \chi_c$. The main effect of increasing the surface periodicity d_x with respect to d_0 is to stabilize tilted lamellae, with increasing tilt angle. Note that even for $d_x = d_0$ [Fig. 5a] yielding no tilt, the perpendicular lamellae have a different structure close to the surface as is induced by the surface pattern. Although the surface interactions are assumed to be strictly local, the connectivity of the chains causes surface-bound distortions to propagate into the bulk of the BCP melt. In particular, this is a strong effect in the weak-segregation regime we are considering.

So far in this section we have considered the semi-infinite problem of a BCP melt confined by one patterned surface. It is of experimental and theoretical interest to study thin films of BCP'S when they are confined between a heterogeneous (patterned) surface and a second chemically homogeneous surface. This situation is encountered when a thin BCP film is spread on a patterned

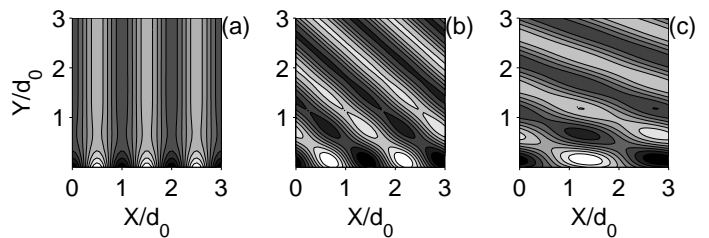


FIG. 6: Tilted lamellar phase in contact with one patterned surface at $y = 0$. (See also Fig. 2c). The surface patterning is modeled by the term $\sigma_q \cos(2\pi x/d_x)$. The lamellae tilt angle $\theta = \arccos(d_0/d_x)$ increases as the periodicity of the surface d_x increases: $\theta = 0$ for $d_x = d_0$ in (a), $\theta \simeq 48.1^\circ$ for $d_x = \frac{3}{2}d_0$ in (b) and $\theta \simeq 70.5^\circ$ for $d_x = 3d_0$ in (c). In the plots $\sigma_q/hq_0^3\phi_L = 1$. The Flory parameter $N\chi = 11.5$ and $\tau_s/hq_0^3 = 0.1$. Adapted from ref [20].

surface. The second interface is the film/air interface and is homogeneous. Usually the free surface has a lower surface tension with one of the two blocks. This bias can be modeled by adding a constant σ_0 term to the $\sigma(x)$ surface field. For simplicity, we assume that the surface at $y = -\frac{1}{2}L$ has purely sinusoidal stripes while at $y = \frac{1}{2}L$ the surface is attractive to one of the A/B blocks with a constant preference:

$$\begin{aligned} \sigma(x) &= \sigma_q \cos(q_x x), & \text{at } y &= -\frac{1}{2}L, \\ \sigma(x) &= \sigma_0, & \text{at } y &= \frac{1}{2}L. \end{aligned} \quad (17)$$

A neutral surface at $y = \frac{1}{2}L$ is obtained as a special case with $\sigma_0 = 0$. The expression (12) for the bulk tilted phase is modified ($y \rightarrow y + \frac{1}{2}L$) in order to match the stripe surface pattern at $y = -\frac{1}{2}L$,

$$\phi_b = -\phi_L \cos \left[q_x x + q_y \left(y + \frac{1}{2}L \right) \right] \quad (18)$$

The homogeneous surface field at $y = \frac{1}{2}L$ induces a lamellar layering parallel to the surface, since the two A/B blocks are covalently linked together. The simplest way to account for this layering effect is to include an x -independent term $w(y)$ in our ansatz, Eq. (14), for the order parameter:

$$\delta\phi(x, y) = g(y) \cos(q_x x) + w(y). \quad (19)$$

The tilted lamellar phase confined by one homogeneous and one patterned surface is a generalization of the mixed (perpendicular and parallel) lamellar phase., which occurs when the surface imposed periodicity d_x is equal to the bulk periodicity d_0 . This “T-junction” morphology, shown in Fig. 7, has perpendicular lamellae extending from the patterned surface. The homogeneous field at the opposite surface favors a parallel orientation of the lamellae. The crossover region between the two orientations is found in the middle of the film, and its morphology depends on temperature (the χ parameter). The

effect of the homogeneous field is evident, as parallel ordering extends from the top surface. We see here that strong enough modulated surface fields stabilize the tilted lamellar phases and, in particular, the mixed phase.

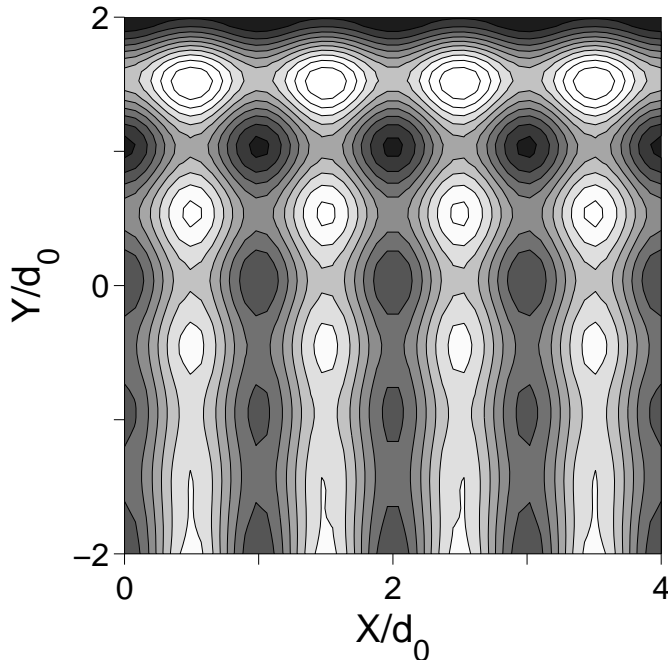


FIG. 7: A BCP confined film showing a crossover from perpendicular lamellae at the $y = -\frac{1}{2}L = -2d_0$ surface to parallel lamellae at the other surface, $y = \frac{1}{2}L$. The pattern on the bottom surface, $\sigma(x) = \sigma_q \cos(q_0 x)$, has the bulk periodicity d_0 , and amplitude $\sigma_q = 2hq_0^3$, while the top surface ($y = \frac{1}{2}L$) is homogeneously attractive to the B polymer (in black), $\sigma_0 = 4hq_0^3$. The Flory parameter is given by $N\chi = 10.7$ and $\tau_s/hq_0^3 = 0.4$. Adapted from ref [20].

BCP'S IN CONTACT WITH ROUGH SURFACES

In the preceding sections we have described how the copolymer morphology is influenced by chemically homogeneous or patterned surfaces that are smooth and flat. Another way to control BCP structure is by the use of rough or corrugated surfaces. This method has some advantages because it is rather straightforward to construct experimentally such surfaces [35]. When a lamellar stacking is placed parallel to a rough, sinusoidally modulated, surface (see Fig. 8), the lamellar state is a compromise between interfacial interactions preferring that the lamellae closely follow the surface contour, and bending and compression energies, preferring flat layers.

The surface roughness is modeled by a single one-dimensional corrugation mode, whose height in the z -direction above an (x, y) reference plane is given by $h(x) = R \cos(q_s x)$. q_s and R are the wavenumber and

amplitude of the surface roughness, respectively (see Fig. 8). The BCP is put above the substrate in the half-space $z \geq h(x)$. We denote γ_{AB} as the interfacial interaction between the A and B blocks in the polymer chain.

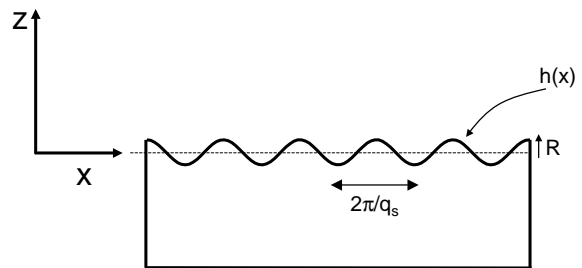


FIG. 8: Schematic illustration of a rough surface, with sinusoidal height undulations $h(x) = h_0 + R \cos(q_s x)$.

For lamellae oriented perpendicular to the surface, the order-parameter is written as [35]:

$$\phi_{\perp}(\mathbf{r}) = \phi_0 \cos(q_0 x + q_0 u(x, z)) \quad (20)$$

The function $u(x, z)$ describes the surface-induced deviation of the A/B interface from its flat (perfect) shape. The bulk part of the free energy can be written as [36, 37, 38]:

$$F_b = \frac{1}{2} \int [K(u_{zz})^2 + B(u_x)^2] d^3 r \quad (21)$$

where $u_x = \partial u / \partial x$, $u_{zz} = \partial^2 u / \partial z^2$, $K \sim d_0 \gamma_{AB}$ is the bending modulus and $B \sim \gamma_{AB} / d_0$ is the compression modulus. To the elastic energy integral above must be added a term taking into account the interfacial energies of the A and B blocks. This is simply given by $\frac{1}{2}(\gamma_{AS} + \gamma_{BS})$, multiplied by a correction factor. This factor is $1 + \frac{1}{4}(q_s R)^2$, reflecting the fact that the real surface area is larger than the projected one, and assuming small roughness $q_s R \ll 1$. Minimization of the free-energy above gives the expression for u . The deformation u is larger close to the surface, as can be seen from the deformation of the perpendicular lamellae in Figure 9 (a).

Substitution of the expression for u back into the free-energy integral Eq. (21) gives the free-energy per unit area of the perpendicular lamellae

$$F_{\perp} \simeq \phi_0^2 \frac{(\gamma_{AS} - \gamma_{BS})^2}{q_0 K} + \frac{1}{2} (\gamma_{AS} + \gamma_{BS}) \left(1 + \frac{1}{4} (q_s R)^2 \right) \quad (22)$$

The deformation u for parallel lamellae can be achieved in a similar way. The resulting parallel layering is seen

in Fig. 9 (b), with the same parameters as in part (a). The total free-energy in this case is:

$$F_{\parallel} \simeq \phi_0^2 \frac{(\gamma_{AS} - \gamma_{BS})^2}{q_0 K} \left(\frac{q_0}{q_s} \right)^2 (q_0 R)^2 + \left[\left(\frac{1}{2} - \phi_0 \right) \gamma_{AS} + \left(\frac{1}{2} + \phi_0 \right) \gamma_{BS} \right] \left(1 + \frac{1}{4} (q_s R)^2 \right) \quad (23)$$

Here again we find the same factor $1 + \frac{1}{4} (q_s R)^2$, but the energies of interaction with the surface are different from the previous case: the A and B polymers do not cover the surface equally, and hence γ_{AS} and γ_{BS} have different prefactors in the square brackets.

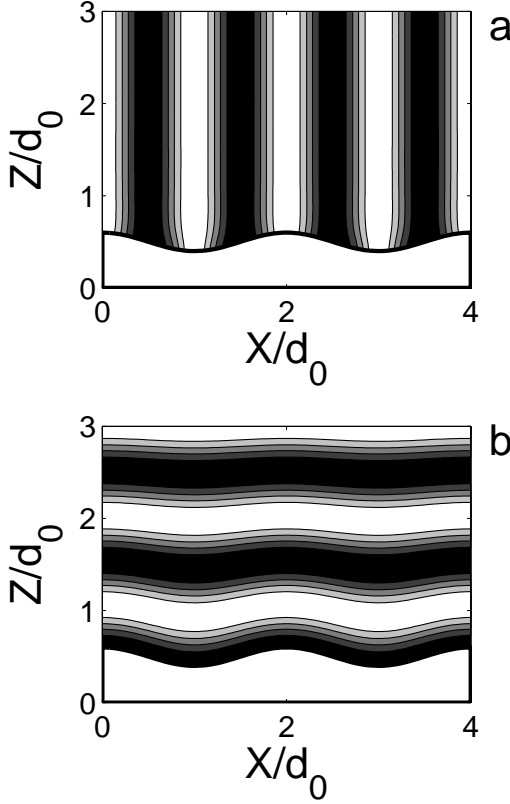


FIG. 9: Perpendicular (a) and parallel lamellae (b) on rough surfaces. The lamellar periodicity is half the surface one. The parameters used are $B = 2 \times 10^5 \text{ J/m}^2$, $K = B/(4q_0^2)$ and $\sigma = \gamma_{AS} - \gamma_{BS} = \sqrt{BK}/4$. Adapted from ref [35].

Based on the free-energies above, Eqs. (22) and (23), a phase diagram can be constructed in the phase space of three variables: the surface and lamellar inverse periodicities q_s and q_0 , respectively, and the surface amplitude R . Three cuts in the phase diagram are given in Fig. 10. In (a), R and q_s are scaled by q_0 . An increase in q_s while keeping q_0 and R constant generally leads to a preference of parallel layering. A different view is presented in (b), where q_0 and R are scaled by q_s . Here, keeping q_s and

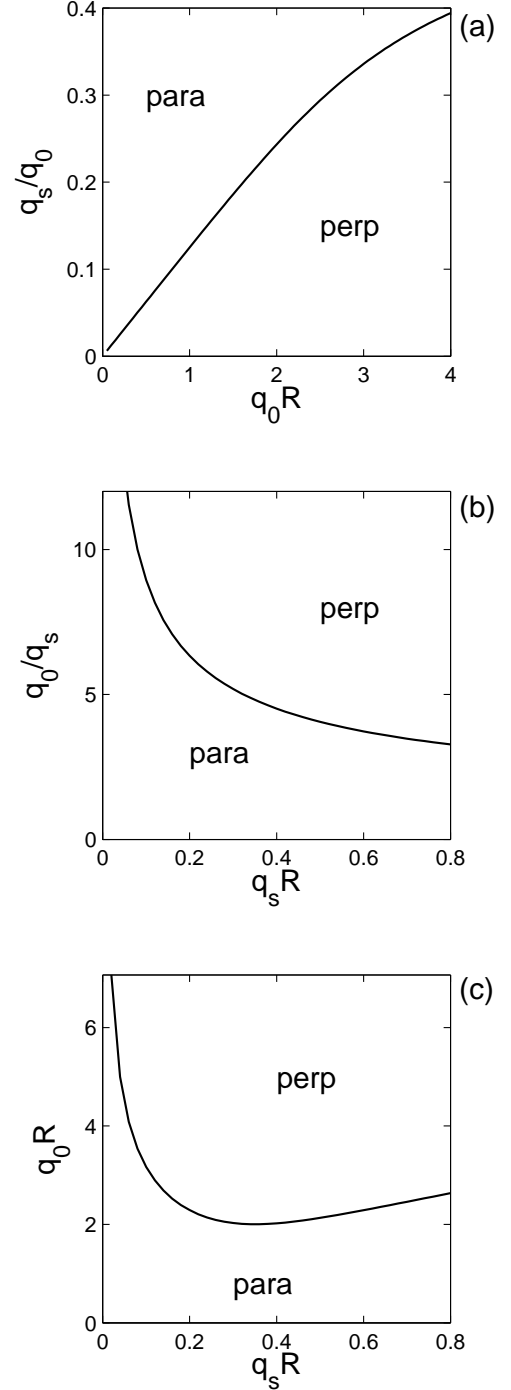


FIG. 10: Phase-diagrams for perpendicular and parallel lamellar on roughs substrates. (a) R and q_s are scaled by q_0 . (b) The surface wavenumber q_s is used to scale q_0 and R . (c) q_s and q_0 are scaled by the surface amplitude R . In the three plots we used $\phi_0 = 0.4$. The parameters used are $\sigma = \gamma_{AS} - \gamma_{BS} = 0.25 \text{ mN/m}$ and $\gamma_{AB} = 1 \text{ mN/m}$. Adapted from ref [36]

q_0 fixed while increasing R leads to a preference of perpendicular ordering. Similarly, in (c) R is used to scale q_s and q_0 . An increase of q_0 at constant q_s and R favors

perpendicular lamellae.

In the preceding sections we have considered ordering mechanisms where the interaction of the polymers with the confining surfaces is mediated to regions far from the surfaces because of chain connectivity. We now turn to discuss orientation of BCP films in presence of external electric fields. This is a bulk ordering mechanism that does not originate from the surface.

BCP'S IN PRESENCE OF ELECTRIC FIELDS

The influence that an electric field has on anisotropic polarizable media (e.g. block copolymers) is of great importance. We will, in particular, concentrate on two aspects: orientational transitions and order-to-order phase transitions.

Orientation of anisotropic phases by an electric field

When a material with inhomogeneous dielectric constant is placed in an electric field E , there is an electrostatic free energy penalty for having dielectric interfaces perpendicular to the field [39, 40, 41, 42, 43, 44, 45, 46]. This is the so-called “dielectric mechanism” for BCP orientation. Thus, a state where $\nabla\epsilon$ is perpendicular to the field \mathbf{E} is favored [47]. The strength of this effect is proportional to $(\epsilon_A - \epsilon_B)^2 E^2$, where ϵ_A and ϵ_B are the dielectric constants of the polymers, and is enhanced when the difference in polarizabilities is large.

Consider BCP in the lamellar phase and confined between two flat and parallel electrodes. The lamellae may order parallel to the surfaces and suffer some unfavorable stretching or compression, in order to gain better surface coverage, as is discussed in the preceding sections. An applied electric field perpendicular to the surface will tend to orient the lamellae parallel to it, provided that it can overcome the interfacial interactions. In the weak-segregation regime ($\phi \ll 1$), the electrostatic energy per unit volume is given by the Amundson-Helfand approximation [40, 41]

$$F_{\text{es}} = \frac{(\epsilon_A - \epsilon_B)^2}{2\bar{\epsilon}} \sum_q (\hat{\mathbf{q}} \cdot \mathbf{E})^2 \phi_{\mathbf{q}}^2 \quad (24)$$

where the sum is taken over all q -modes in the expression $\phi(\mathbf{r}) = \sum_{\mathbf{q}} \phi_{\mathbf{q}} \cos(\mathbf{q} \cdot \mathbf{r})$, and $\bar{\epsilon} = f\epsilon_A + (1-f)\epsilon_B$ is the average dielectric constant. A proper ansatz for the copolymer morphology is a linear combination of parallel and perpendicular layering: $\phi(\mathbf{r}) = w(E)\phi_{\parallel}(\mathbf{r}) + g(E)\phi_{\perp}(\mathbf{r})$, with field-dependent amplitudes $w(E)$ and $g(E)$. When this ansatz is substituted into the free-energy, the amplitudes can be calculated and the order-parameter obtained.

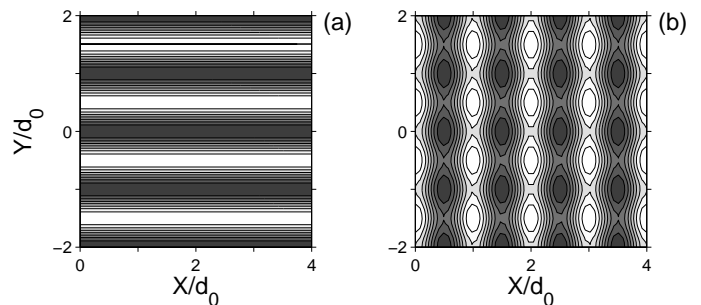


FIG. 11: Lamellar layers of BCP's between two surfaces and under external electric field. The surfaces are at $y = \pm 2d_0$, and the field is in the y direction. The B monomers (colored black) are attracted to both surfaces. (a) The field is slightly smaller than the critical field, $E = 0.98E_c$, and the film has a perfect parallel ordering. (b) The field is just above the threshold, $E = 1.02E_c$. The film morphology is a superposition of parallel and perpendicular lamellae. Adapted from ref [39].

Figure 11 shows the resulting BCP morphology under external electric field oriented perpendicular to the surfaces [39]. In (a) the field is just below a *critical field* and the lamellae lie parallel to the electrodes. However, when the field is increased just above the critical field, a transition occurs to a highly distorted but predominantly perpendicular layering [see (b)]. As the field further increases, the modulations diminish and the lamellae achieve perfect ordering perpendicular to the surfaces.

In Fig. 11(b), it is clear that the surface effect propagates far into the bulk, as the copolymer modulations persist throughout the whole film. In the strong-segregation regime, however, this is not true, and the surface effect is localized. We thus can imagine a third morphology, that of a “mixed” phase. In this morphology few parallel lamellae exist near the surfaces, while the rest of the film is in the perpendicular orientation. A “T-junction” defect is therefore created, and a surface-tension term γ_T must be associated with it. Indeed such a morphology has been visualized lately by Russell and co-workers [50].

The phase diagram in the plane of δ and E is shown in Figure 12 (a), where $\delta \equiv (\gamma_{AS} - \gamma_{BS})/\gamma_T$, for fixed surface separation [39]. There exist three fields E_1 , E_2 and E_3 separating the parallel, perpendicular and mixed orientations. At small fields, there is a direct transition from parallel to perpendicular layers as the field is increased. The mixed state is only possible above a certain threshold of δ , δ^* . Above this threshold, the mixed state is stable at fields larger than E_1 but smaller than E_2 . An increase of E above E_2 leads to the stability of perpendicular lamellae.

The phase diagram in the L and E plane is shown in Figure 12 (b), for a fixed value of δ . At small surface separations, an increase of E leads to a transition from

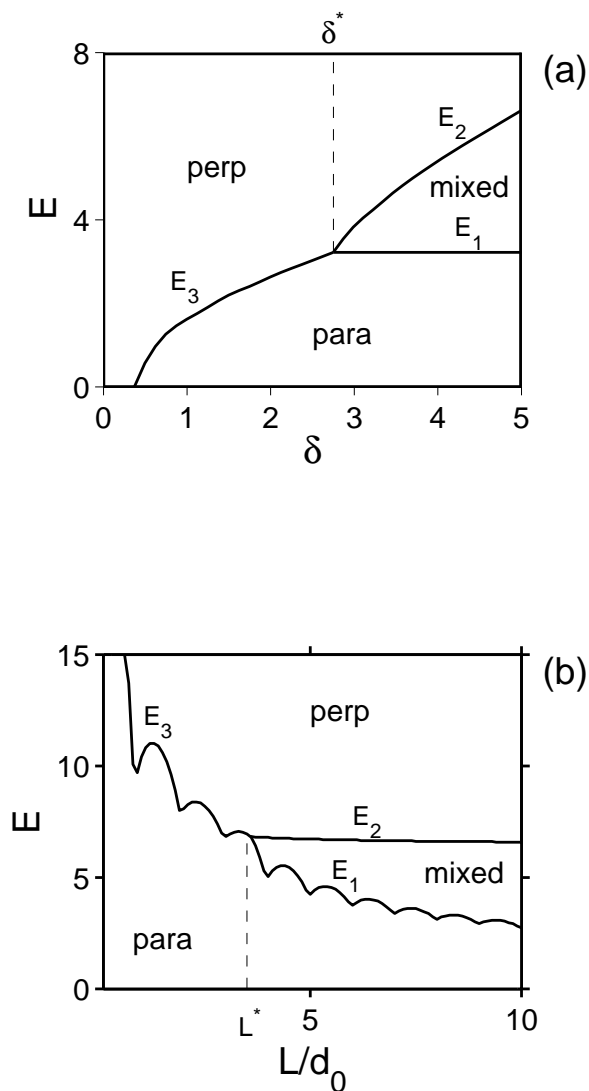


FIG. 12: (a) Phase diagram in the E - δ plane. When $\delta = (\sigma_{AS} - \sigma_{BS})/\gamma_T < \delta^*$, there is a transition between parallel and perpendicular lamellae at $E = E_3$. At larger δ , $\delta > \delta^*$, the transition to the mixed state is followed by a second transition to the perpendicular state when $E = E_2$. The surface separation is chosen as $L = 10d_0$. (b) Similar diagram, but in the E - L plane, with $\delta = 5$. Adapted from ref [39].

parallel to perpendicular lamellae at $E = E_3$. At surface separations larger than a threshold value L^* , increase of E above E_1 leads to a mixed morphology, whereas further increase above E_2 gives rise to perpendicular lamellae.

Phase transitions in electric fields

Orientation of anisotropic phases occurs when the ordered phase has some freedom to rotate, and when the applied electric fields are not too high. However electric

fields can cause a phase transition in systems composed of several components with different dielectric constants [51]. If the BCP phase under consideration cannot rotate in order to reduce the electrostatic energy, it begins to deform. A gradual change then occurs - this is usually an elongation of domain in the direction parallel to the field. At a certain point, it is more favorable for the system to make a drastic change in symmetry and “jump” to the state with the best (i.e. minimal) electrostatic energy [51, 52]. This kind of phase transition is expected to occur at relatively high fields for BCP’s, $E \sim 50 - 100$ V/ μm , so sometimes the phase transition is preempted by dielectric breakdown of the material.

As an example of such a phase transition consider diblock copolymers in the bcc phase of spheres, under an electric field \mathbf{E} . To the lowest (quadratic) order in ϕ , the electrostatic energy is given by the Amundson-Helfand expression Eq. (24). Higher order expressions are available as well [53]. At very high fields, the spheres will elongate into cylinder oriented along the field, which can be assumed to lie in the (1, 1, 1) direction of the lattice. The transition from perfect bcc to hexagonal symmetries of ϕ can be achieved by the following ansatz [52]:

$$\phi(\mathbf{r}, \mathbf{E}) = w(E) \sum_{n=1}^3 \cos(\mathbf{q}_n \cdot \mathbf{r}) + g(E) \sum_{m=4}^6 \cos(\mathbf{q}_m \cdot \mathbf{r}) \quad (25)$$

where

$$\begin{aligned} \mathbf{q}_{1,4} &= q_0(\mp 1, 0, 1)/\sqrt{2} \\ \mathbf{q}_{2,5} &= q_0(1, \mp 1, 0)/\sqrt{2} \\ \mathbf{q}_{3,6} &= q_0(0, 1, \mp 1)/\sqrt{2} \end{aligned} \quad (26)$$

At zero electric field, $w(E) = g(E)$ and ϕ represents a bcc phase. For large enough field the order parameter reduces to the hexagonal one: $g(E) = 0$, and $\phi_{\text{hex}}(\mathbf{r}) = A_{\text{hex}} \sum_{n=1}^3 \cos(\mathbf{q}_n \cdot \mathbf{r})$.

The result of the minimization of $F = F_b + F_{\text{es}}$ gives the value of $w(E)$ and $g(E)$ and therefore ϕ . Figure 13 (a) shows the BCP morphology in the absence of field. As the field is increased, the spheres deform and elongate along the external field. This state represents a compromise between electrostatic energy and stretching of the polymer chains. There exist a critical field E_c above which a direct transition to cylinders occurs: in (b) the field is $E = 0.98E_c$, while in (c) the field is just above the critical one ($E = 1.02E_c$), and perfect cylinders are formed.

The complete phase diagram taking into account the relative stability of the various meso-phases can be calculated. We have done so by two mean-field methods: the first is an analytical method based on the above coarse-graining approach. The second one is a more rigorous treatment based on numerical solutions of self-

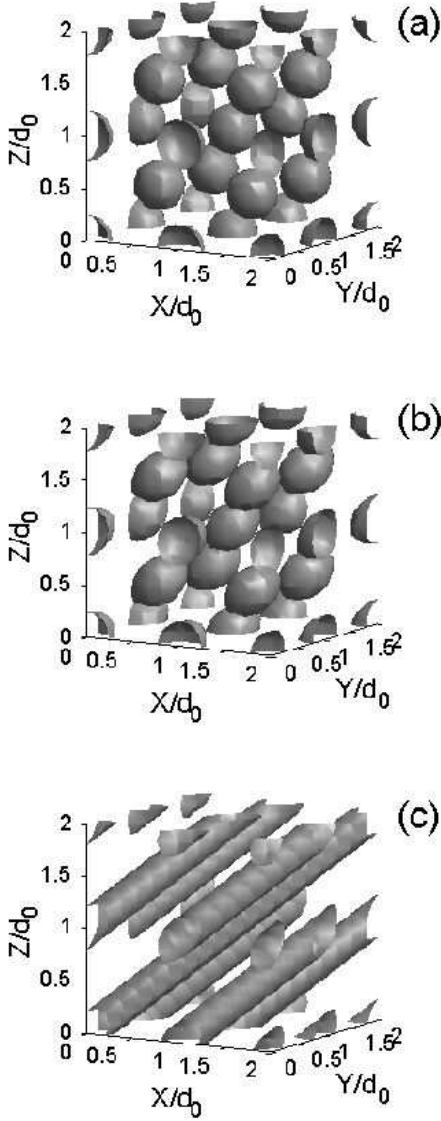


FIG. 13: Cubic phase of block copolymers in electric field. (a) Electric field is $E = 0$. (b) $E = 0.98E_c$, just 2% below the critical field, and oriented along the $(1, 1, 1)$ direction of the lattice. The spheres are deformed. (c) $E = 1.02E_c$, just above the critical field, and the system undergoes an abrupt change into the hexagonal array of cylinders. Adapted from ref [52]

consistent field equations for the copolymer concentration [53]. The result is shown in Figure 14 in the plane of field E and Flory parameter χ , and for a particular composition $f = 0.3$. The distorted bcc phases, denoted as $R\bar{3}m$, is bounded by the hexagonal (hex) and disordered (dis) phases. All three meet at a triple point $(E_t, \chi_t) = (0.49, 14.11/N)$, where fields are scaled by $\hat{E}_0 \equiv (\varepsilon_0 v_p / k_B T)^{1/2}$, where ε_0 is the vacuum permittivity and v_p is the volume of one copolymer chain.

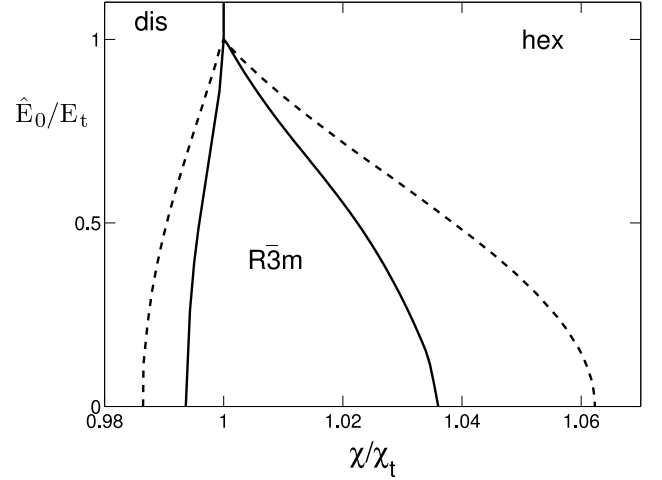


FIG. 14: Phase-diagram of block copolymers in electric field, in the plane of the Flory parameter χ and normalized electric field \hat{E}_0 . The distorted bcc phase, denoted as $R\bar{3}m$, is bounded by the hexagonal (hex) and disordered (dis) phases. Solid line is the prediction of analytical one-mode approximation, whereas dashed lines are obtained by a more accurate self-consistent numerical study. Axes are scaled by (χ_t, E_t) , the values of χ and \hat{E}_0 at the triple point. Adapted from ref [53].

Ionic impurities in BCP's

The above discussion pertains to somewhat “ideal” polymers, because in the electric response only their dielectric constant was considered. However, most polymers are prepared by anionic polymerization. The process is initiated by one ButylLithium ion (BuLi). After rinsing with water, the loose Li binds with an OH group to form LiOH, some of which are dissociated. Hence, there is a finite number of positive and negative ions in the material, and their presence changes the system behavior.

The existence of dissociated ions means that there are additional *forces* which act in the alignment process of the BCP meso-phases. These forces depend on the mobility μ of the ions, and on the frequency ω of applied field. The torque due to mobile ions is expected to be large if the drift velocity $\pi e \mu E / \omega$ is larger than the BCP domain size d_0 . In addition, mobile charges also mean that there is *dissipation*. Hence, the energy stored in the dielectric medium εE^2 should be compared to the Joule heating in one cycle of the field $2\pi\sigma E^2 / \omega$, where σ is the ions conductivity, proportional to the ion density. It is clear from the above that for low frequencies (in practice $\lesssim 100$ Hz) mobile dissociated ions begin to play an important role in BCP alignment and phase transitions [54].

When the additional complexity due to these ions is taken into account, it turns out that the orientation forces (torques) due to the mobile ions scale as $1/\omega$ [54], and

are equal to the ones due to the regular “dielectric mechanism” at about 50 Hz. Consequently they are twice as large at 25 Hz, and they become more important as the frequency is reduced.

Taking into account the effect of mobile ions on the BCP phase transition as outlined above (from bcc phase of spheres to a hexagonal array of cylinders), it turns out that the transition field E_c can be significantly reduced from a value of $\approx 70\text{-}100\text{ V}/\mu\text{m}$ to values $\sim 20\text{ V}/\mu\text{m}$ [52].

CONCLUSIONS

We review in this paper several ordering mechanisms in confined BCP’s. The theoretical approach relies on a mean-field coarse-grained Hamiltonian, which is less sensitive to microscopic details and valid for a wide class of system showing self-assembly in soft-matter. This approach thus complements other computationally-intensive self-consistent numerical schemes [25, 26, 27, 55, 56] and Monte-Carlo simulations [57, 58, 59, 60]. The polymer density near a chemically patterned surface is given above the order-disorder temperature as a function of the surface pattern. In this regime the chemical pattern q -modes give rise to density modes which are decoupled from each other (linear response theory). In the weak segregation regime, the surface correlations are long range and, therefore, simple chemical patterns yield complex copolymer morphology, even though the bulk is in its disordered phase.

Below the ODT temperature, we consider lamellae confined by homogeneous surfaces, and examine the relative stability of parallel vs. perpendicular ordering as a function of temperature, surface separation and interfacial interactions. Lamellae confined by striped surface whose periodicity is larger than the lamellar periodicity appear tilted with respect to the surface thereby optimizing their surface interactions. The lamellar undulations are more prominent as the ODT is approached. Mixed lamellar phases appear when one surface has chemically patterns in the form of stripes while the other is uniform.

A different paradigm for control of BCP orientation in thin films is using rough surfaces. This method may be advantageous over other methods in several situations since it is relatively simple to implement experimentally. The phase diagram is presented for the ordered phases as a function of surface period, surface amplitude, and lamellar period, as well as other parameters.

Lastly, the influence of electric field on the phase behavior of BCP’s is considered. An external electric field favors a state where dielectric interfaces are perpendicular to the field itself. Hence, lamellae confined in a thin-film are electrostatically preferred perpendicular rather than parallel to the confining electrodes. In the weak-segregation regime, there is one critical field at which parallel layers are transformed into perpendicular ones.

Even for fields larger than the critical field, the long-range effect of the surfaces is evident as strong lamellar undulations. The strong segregation regime is considered as well. Here we find three possible states: parallel, perpendicular and mixed. The last morphology exhibits few parallel layers close to the electrodes while the rest of the film is perpendicular. There are either two or one critical fields separating them, depending on the interfacial interactions.

An external electric field can also bring about a phase transition in ordered phases, if they are frustrated and cannot eliminate dielectric interfaces perpendicular to the field direction. The transition from the bcc phase of spheres to a hexagonal array of cylinders under the influence of electric field is discussed as an example. Below the critical field the spheres elongate in the field’s direction, but above it we find perfect cylinder whose axes are parallel to the field. The phase diagram of the various meso-phases is calculated, and the simple analytical expression obtained with the coarse-graining theory is compared with a more rigorous SCF theory, with rather good match. We point out that residual dissociated ions in BCP’s can greatly enhance the electric field effect, and this is specially true in low-frequency electric fields.

The analytical calculations presented here rely on a relatively simple mean-field coarse-grained free-energy functional. This approach allowed us to deal with confinement effects in BCP, take into account the chemical nature of the surfaces, calculate the elastic energy penalty and lamellar conformation near curved interfaces and balance the electrostatic energy against the elastic one for BCP’s in electric fields. The coarse-grained approach has a big advantage that it can be generalized and account for other complex polymer systems. Because it is less accurate in terms of quantitative predictions, it is useful to compare this approach with numerical self-consistent field theories, discrete lattice models, Monte-Carlo and molecular dynamics simulations and experiments.

Acknowledgments

Our research on block copolymer have been conducted in collaboration with T. Hashimoto, L. Leibler, C.-Y. Lin, M. Schick, E. Sivaniah and F. Tournilhac. We would like to thank K. Binder, Y. Cohen, G. Fredrickson, S. Gido, G. Krausch, M. Muthukumar, T. Ohta, G. Reiter, T. P. Russell, U. Steiner, I. Szleifer, E. Thomas, T. Thurn-Albrecht, M. Turner and T. Xu for numerous discussions. This research is partly supported by the Israel Science Foundation (ISF) under grant No. 160/05 and the US-Israel Binational Foundation (BSF) under grant No. 287/02.

-
- [1] Hamley, I. W. in *The Physics of Block Copolymers*, Oxford University: Oxford, 1998.
- [2] Bates, F. S.; Fredrickson, G. H. *Physics Today* 1999, February, 32.
- [3] Cohen, Y.; Albalak, R. J.; Dair, B. J.; Capel, M. S.; Thomas, E. L. *Macromolecules* 2000, 33, 6502.
- [4] Cohen, Y.; Brinkmann M.; Thomas, E. L. *J Chem Phys* 2001, 114, 984.
- [5] Chen, Z.-R.; Kornfield, J. A.; Smith, S. D.; Grothaus, J. T.; Satkowski, M. M. *Science* 1997, 277, 1248.
- [6] Vlasov, Y. A.; Bo, X. Z.; Sturm, J. C.; Norris, D. J. *Nature* 2001, 414, 289.
- [7] Fink, Y.; Winn, J. N.; Fan, S.; Chen, C.; Michel, J.; Joannopoulos, J. D.; Thomas, E. L. *Science* 1998, 282, 1679.
- [8] Khandpur, A. K.; Foerster, S.; Bates, F. S.; Hamley, I. W.; Ryan, A. J.; Bras, W.; Almdal, K.; Mortensen, K. *Macromolecules* 1995, 28, 8796.
- [9] Leibler, L. *Macromolecules* 1980, 13, 1602.
- [10] Binder, K.; Frisch, H. L.; Stepanow, S. *J Phys. II* 1997, 7, 1353.
- [11] Fredrickson, G. H.; Helfand, E. *J Chem Phys* 1987, 87, 697.
- [12] Ohta, T.; Kawasaki, K. *Macromolecules*, 1986, 19, 2621.
- [13] Tsori, Y.; Andelman, D. *Europhys Lett* 2001, 53, 722.
- [14] Swift, J.; Hohenberg, P. C. *Phys Rev A* 1997, 15, 319.
- [15] Bates F. S.; Fredrickson, G. H. *Annu Rev Phys Chem* 1990, 41, 525.
- [16] Brazovskii, S. A. *Sov Phys JETP* 1975, 41, 85.
- [17] Kellogg, G. J.; Walton, D. G.; Mayes A. M.; Lambooy, P.; Russell, T. P.; Gallagher P. D.; Satija, S. K. *Phys Rev Lett* 1996, 76, 2503.
- [18] Mansky, P.; Russell, T. P.; Hawker, C. J.; Mayes, J.; Cook, D. C.; Satija, S. K. *Phys Rev Lett* 1997, 79, 237.
- [19] Fredrickson, G. H. *Macromolecules* 1987, 20, 2535.
- [20] Tsori, Y.; Andelman, D. *J Chem Phys* 2001, 115, 1970.
- [21] Tsori, Y.; Andelman, D. *Interface Sci.* 2003, 11, 259.
- [22] Tsori, Y.; Andelman, D. *Macromolecules* 2001, 34, 2719.
- [23] Walton, D. G.; Kellogg, G. J.; Mayes, A. M.; Lambooy, P.; Russell, T. P. *Macromolecules* 1994, 27, 6225.
- [24] Turner, M. S. *Phys Rev Lett* 1992, 69, 1788.
- [25] Matsen, M. W. *J. Chem. Phys.* 1997, 106, 7781.
- [26] Matsen, M. W.; Bates, F. S. *J. Chem. Phys.* 1997, 106, 2436.
- [27] Pickett G. T.; Balazs, A. C. *Macromolecules* 1997, 30, 3097.
- [28] Geisinger, T.; Mueller M.; Binder, K. *J Chem Phys* 1999, 111, 5241.
- [29] Wang, Q.; Yan, Q.; Nealey, P. F.; de Pablo, J. J. *J Chem Phys* 2000, 112, 450.
- [30] Pereira, G. G.; Williams, D. R. M. *Macromolecules* 1999, 32, 1661; *ibid*, 1999, 32, 758.
- [31] Wang, Q.; Nath, S. K.; Graham, M. D.; Nealey P. F.; de Pablo, J. J. *J Chem Phys* 2000, 112, 9996.
- [32] Tsori, Y.; Andelman, D. *Eur Phys J E* 2001, 5, 605.
- [33] Heier, J.; Kramer, E. J.; Walheim, S.; Krausch, G. *Macromolecules* 1997, 30, 6610.
- [34] Tsori, Y.; Andelman, D.; Schick, M. *Phys Rev E* 2000, 61, 2848.
- [35] Tsori, Y.; Andelman, D. *Macromolecules* 2003, 36, 8560.
- [36] Tsori, Y.; Sivaniah, E.; Andelman, D. Hashimoto, T. *Macromolecules* 2005, 38, 7193.
- [37] Turner, M. S.; Joanny, J.-F. *Macromolecules* 1992, 25, 6681.
- [38] de Gennes, P.-G.; Prost, J. *The Physics of Liquid Crystals*, 2nd Edition ; Oxford University Press: Oxford, 1993.
- [39] Tsori, Y.; Andelman, D. *Macromolecules* 2002, 35, 5161.
- [40] Amundson, A.; Helfand, E.; Quan, X.; Hudson, S. D. *Macromolecules* 1993, 26, 2698.
- [41] Amundson, K.; Helfand, E.; Quan, X. *Macromolecules* 1994, 27, 6559.
- [42] Onuki, A.; Fukuda, J. *Macromolecules* 1995, 28, 8788.
- [43] Pereira, G. G.; Williams, D. R. M. *Macromolecules* 1999, 32, 8115
- [44] Ashok, B.; Muthukumar, M.; Russell, T. P. *J Chem Phys* 2001, 115, 1559.
- [45] Thurn-Albrecht, T.; DeRouchey, J.; Russell, T. P. *Macromolecules* 2000, 33, 3250.
- [46] Kyrlyuk, A. V.; Zvelindovsky, A. V.; Sevink G. J. A.; Fraaije, J. G. E. M. *Macromolecules* 2002, 35, 1473.
- [47] Böker, A.; Knoll, A.; Elbs, H.; Abetz, V.; Müller, A. H. E.; Krausch, G. *Macromolecules* 2002, 35, 1319.
- [48] Böker, A.; Schmidt, K.; Knoll, A.; Zettl. H.; Hansel, H.; Urban, V.; Abetz, V.; Krausch, G. *Polymer* 2006, 47,849.
- [49] Böker, A.; Elbs, H.; Hansel, H.; Knoll, A.; Ludwigs, S.; Zettl, H.; Zvelindovsky, A. V.; Sevink, G. J. A.; Urban, V.; Abetz, V.; Müller, A. H. E.; Krausch, G. *Macromolecules* 2003, 36, 8078.
- [50] Xu, T.; Hawker, C. J.; Russell, T. P. *Macromolecules* 2005, 38, 2802.
- [51] Tsori, Y.; Tournilhac, F.; Leibler, L. *Nature* 2004, 430, 544.
- [52] Tsori, Y.; Tournilhac, F.; Andelman, D.; Leibler, L. *Phys Rev Lett* 2003, 90, 145504.
- [53] Tsori, Y.; Andelman, D.; Lin, C.-Y.; Schick, M. *Macromolecules* 2006, 39, 289.
- [54] Tsori, Y.; Tournilhac, F.; Leibler, L. *Macromolecules* 2003, 36, 5873.
- [55] Shull K. R. *Macromolecules* 1998, 31, 5904.
- [56] Matsen, M. W.; Schick, M. *Phys. Rev. Lett.* 1994, 72, 2660.
- [57] Binder, K. *Acta Polymer.* 1995, 46, 204.
- [58] Binder, K. *Top. Appl. Phys.* 1995, 71, 355.
- [59] Szleifer, I.; Loring, R. F. *J. Chem. Phys.* 1994, 100, 5367.
- [60] Szleifer, I. *Curr. Opin. Colloid. Sci.* 1996, 1, 416.